

Sedimentation of a Solid Particle Immersed in a Fluid Film

A. Sellier¹ and L. Pasol²

Abstract: This paper examines the slow viscous settling migration of a solid particle immersed in a viscous fluid film confined by two plane and parallel solid wall and free surface. The approach rests on the use of suitable boundary-integral equations on the surface of the particle and the analytical calculation of a new Green tensor that complies with all the boundary conditions satisfied by the liquid flow on the plane boundaries. The numerical implementation resorts to standard boundary elements on the particle's surface and provides at a reasonable cpu time cost the motion of the particle and, if necessary, the velocity field in the liquid film. The migration of a sphere is found to deeply depend on its location, the gravity field and the fluid film thickness. Depending on these parameters the sphere may either translate faster, slower or at the same speed than in absence of boundaries. This latter case arises at a critical location of the sphere for a gravity field parallel to the boundaries.

keyword: Sedimentation, fluid film, wall-particle interactions, free surface-particle interactions, Green tensor, boundary-integral equations.

1 Introduction

The motion of solid particles immersed in a thin film fluid bounded by a plane solid wall and a free surface admits many industrial applications such as photographic coating. Hence, Li and Pozrikidis (2003) recently investigated the viscous two-dimensional gravity-driven film flow of a suspension of 2D solid particles and computed, within this framework, the deformation of the interface. Since particles are in practice three-dimensional it however remains of prime interest to tackle the challenging case of a collection of three-dimensional particles. Even for a single particle the available works (see Ganatos, Peffer, and Weibaum (1980a), Ganatos, Peffer, and Weibaum (1980b), Staben, Zinchenko, and Davis (2003)) consider two plane and parallel solid bound-

aries and the case of two parallel plane solid wall and free surface has not been addressed so far. The present work therefore introduces a new approach to compute the gravity-driven rigid-body motion of a 3D and arbitrarily-shaped particle in a fluid film confined by two plane and parallel solid wall and free surface and may be seen as the first step towards modelling the rheology of dilute fully three-dimensional suspension film flows. This is achieved by establishing a boundary-integral formulation of the problem and analytically obtaining the Green tensor which complies with all the boundary conditions.

The paper is organized as follows. The governing problem and the relevant boundary-integral equations are presented in §2 whereas the determination of the associated Green tensor is addressed in §3. The numerical implementation and several results for the sedimentation of a spherical particle are presented in §4 whereas a few concluding remarks are given in §5.

2 Governing linear system and boundary-integral equations

This section introduces our assumptions and shows how it is possible to compute within this framework the settling motion of the particle by solely solving six Fredholm boundary-integral equations on the particle's surface. By the way we indicate how to subsequently determine,

if necessary, the induced liquid velocity field by exploiting a fruitful integral representation of the flow valid in the entire fluid domain.

2.1 Assumptions and governing equations

We consider, as sketched in Fig. 1, a solid particle \mathcal{P} immersed in a quiescent Newtonian viscous fluid with uniform density ρ and viscosity μ . The particle, not necessarily homogeneous, has density ρ_s , volume \mathcal{V} , center of mass O' and center of volume O'' . The fluid is confined between the motionless plane solid wall $\Sigma_1(x_3 = -W)$ and the undisturbed plane free surface $\Sigma_2(x_3 = W)$. Both the fluid and the particle \mathcal{P} are subject to a uniform

¹ LadHyX, Ecole Polytechnique, FRANCE

² LPT, Espci, Paris, FRANCE.

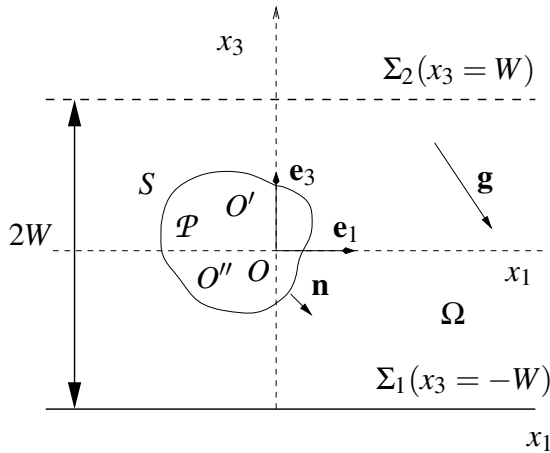


Figure 1 : A solid particle \mathcal{P} immersed in a fluid film and subject to the uniform gravity field \mathbf{g} . The film thickness is $2W$ with $W > 0$.

gravity field \mathbf{g} and this results in a rigid-body motion of \mathcal{P} with unknown translational velocity \mathbf{U} (the velocity of O') and angular velocity ω with respect to Σ_1 and a liquid flow with unknown velocity \mathbf{u} and pressure $p + \rho\mathbf{g}\cdot\mathbf{OM}$ at any point M in the liquid domain Ω . In theory the upper free surface Σ_2 should be disturbed. However, we henceforth neglect this deformation and assume that Σ_2 remains flat. This model is actually valid in practice as soon as the particle lies far enough from the free-surface or when either the surface tension or the liquid density is large (see Lee, Chadwick, and Leal (1979)). Note that in other circumstances this zeroth-order solution would subsequently permit us to gain, if necessary, the small but not negligible deformation of the free-surface by proceeding as explained in Lee, Chadwick, and Leal (1979). If \mathcal{P} has length scale a and \mathbf{u} has typical magnitude U we further assume that $\text{Re} = \rho U a / \mu \ll 1$ and neglect all inertial effects. Under those assumptions the liquid experiences a quasi-steady low-Reynolds-number flow (\mathbf{u}, p) , with stress tensor σ , obeying the following problem

$$\mu \nabla^2 \mathbf{u} = \nabla p \text{ and } \nabla \cdot \mathbf{u} = 0 \text{ in } \Omega, \quad (1)$$

$$(\mathbf{u}, p) \rightarrow (\mathbf{0}, 0) \text{ as } |\mathbf{OM}| \rightarrow \infty, \quad (2)$$

$$\mathbf{u} = \mathbf{0} \text{ on } \Sigma_1, \mathbf{u} \cdot \mathbf{e}_3 = \mathbf{e}_1 \cdot \sigma \cdot \mathbf{e}_3 = \mathbf{e}_2 \cdot \sigma \cdot \mathbf{e}_3 = 0 \text{ on } \Sigma_2, \quad (3)$$

$$\mathbf{u} = \mathbf{U} + \omega \wedge \mathbf{O}'\mathbf{M} \text{ on } S \quad (4)$$

where the unit vectors \mathbf{e}_1 and \mathbf{e}_3 are indicated in Fig. 1 and $\mathbf{e}_2 = \mathbf{e}_3 \wedge \mathbf{e}_1$. In (3) we actually require a no-slip boundary condition on the plane solid wall Σ_1 and zero normal velocity and tangential tractions on the steady free-surface Σ_2 whereas the translational and angular velocities \mathbf{U} and ω occurring in (4) are unknown. Because of negligible inertia, the particle experiences zero net force and torque (for instance, with respect to O'). Denoting by \mathbf{n} the unit outward normal on S , we thus supplement (1)-(4) with the relations

$$\int_S \sigma \cdot \mathbf{n} dS = (\rho \mathcal{V} - \mathcal{M}) \mathbf{g}, \quad (5)$$

$$\int_S \mathbf{O}'\mathbf{M} \wedge \sigma \cdot \mathbf{n} dS = \mathcal{M} \mathbf{O}'\mathbf{O}'' \wedge \mathbf{g}. \quad (6)$$

For a prescribed rigid-body motion $\mathbf{X} = (\mathbf{U}, \omega)$ it is thinkable to compute the flow (\mathbf{u}, p) , governed by (1)-(4), by using a 3D Finite Element Code and also to evaluate the resulting traction $\sigma \cdot \mathbf{n}$ on the particle's surface. This suggests determining the rigid-body motion (\mathbf{U}, ω) dictated by (1)-(4) and (5)-(6) by starting with a guess value \mathbf{X}_g and iteratively going on until the conditions (5)-(6) are satisfied. Unfortunately, such a procedure would be highly cpu time consuming and not accurate enough because a loss of accuracy occurs when computing the traction on the particle's surface from the numerical approximation of (\mathbf{u}, p) in it's vicinity. We present in the next subsections a quite different approach which is free from those drawbacks.

2.2 Extended reciprocal identity and resulting key linear system

The key idea here consists in extending and exploiting the reciprocal identity available for Stokes flows. More precisely, let us prove for two arbitrary flows (\mathbf{u}, p) and (\mathbf{u}', p') that obey (1)-(3) with stress tensors σ and σ' the basic identity

$$\int_S \mathbf{u} \cdot \sigma' \cdot \mathbf{n} dS = \int_S \mathbf{u}' \cdot \sigma \cdot \mathbf{n} dS. \quad (7)$$

Using Cartesian coordinates (O, x_1, x_2, x_3) with the notation $d(M) = \{x_1^2 + x_2^2\}^{1/2}$, we first introduce the bounded liquid domain $\Omega(b) = \{M \in \Omega; d(M) \leq b\}$ for b positive and large enough such that the boundary $\partial\Omega(b)$ consists of both S , the cylinder $\Sigma(b) = \{M \in \Omega; d(M) = b\}$ with outward unit normal $\mathbf{n}'(M) = (\mathbf{OM} - x_3 \mathbf{e}_3)/b$ and

surfaces $\Sigma_l(b) = \{M, x_3 = (l-1)W \text{ and } d(M) < b\}$ for $l = 1, 2$. According to the usual reciprocal theorem (see Happel and Brenner (1973)) the equation (1) for (\mathbf{u}, p) and (\mathbf{u}', p') ensures that

$$\int_S [\mathbf{u} \cdot \boldsymbol{\sigma}' - \mathbf{u}' \cdot \boldsymbol{\sigma}] \cdot \mathbf{n} dS = \int_{\Sigma(b)} [\mathbf{u} \cdot \boldsymbol{\sigma}' - \mathbf{u}' \cdot \boldsymbol{\sigma}] \cdot \mathbf{n}' dS + \sum_{l=1}^2 \int_{\Sigma_l(b)} (-1)^l [\mathbf{u}' \cdot \boldsymbol{\sigma} - \mathbf{u} \cdot \boldsymbol{\sigma}'] \cdot \mathbf{e}_3 dS. \quad (8)$$

By virtue of (3) the integrations on the surfaces $\Sigma_l(b)$ appear to vanish. In addition, the far-field behaviors (2) show that the integration on $\Sigma(b)$ vanishes as b becomes large and one thus arrives at (7).

In expressing the conditions (5)-(6) it is fruitful to select (\mathbf{u}', p') as one of the specific Stokes flows $(\mathbf{u}_T^{(i)}, p_T^{(i)})$ or $(\mathbf{u}_R^{(i)}, p_R^{(i)})$ defined for $i = 1, 2, 3$, with stress tensors $\boldsymbol{\sigma}_T^{(i)}$ and $\boldsymbol{\sigma}_R^{(i)}$, and produced by the particle when it translates or rotates respectively parallel to \mathbf{e}_i . In other words, these flows fulfill (1)-(3) and the boundary conditions

$$\mathbf{u}_T^{(i)} = \mathbf{e}_i \text{ and } \mathbf{u}_R^{(i)} = \mathbf{e}_i \wedge \mathbf{O}'\mathbf{M} \text{ on } S. \quad (9)$$

We moreover introduce for $L = T, R$ the traction $\mathbf{f}_L^{(i)} = \boldsymbol{\sigma}_L^{(i)} \cdot \mathbf{n}$ exerted on the particle's surface S by the flow $(\mathbf{u}_L^{(i)}, p_L^{(i)})$ and the associated coefficients

$$A_L^{i,j} = - \int_S \mathbf{e}_j \cdot \mathbf{f}_L^{(i)} dS, \quad B_L^{i,j} = - \int_S (\mathbf{e}_j \wedge \mathbf{O}'\mathbf{M}) \cdot \mathbf{f}_L^{(i)} dS. \quad (10)$$

Adopting henceforth the usual tensor summation convention, it is straightforward by exploiting the identity (7) to cast the relations (5)-(6) into the following 6-equation linear system for the unknown Cartesian velocity components $U_j = \mathbf{U} \cdot \mathbf{e}_j$ and $\Omega_j = \boldsymbol{\omega} \cdot \mathbf{e}_j$

$$A_T^{i,j} U_j + B_T^{i,j} \Omega_j = (\mathcal{M} - \rho \mathcal{V}) \mathbf{g} \cdot \mathbf{e}_i, \quad (11)$$

$$A_R^{i,j} U_j + B_R^{i,j} \Omega_j = \mathcal{M} (\mathbf{g} \wedge \mathbf{O}'\mathbf{O}'') \cdot \mathbf{e}_i. \quad (12)$$

In order to prove that (11)-(12), with 6×6 matrix \mathbf{A} , admits a unique solution let us consider for 6 arbitrary real numbers T_i and R_i the flow (\mathbf{u}', p') such that

$$\mathbf{u}' = T_i \mathbf{u}_T^{(i)} + R_i \mathbf{u}_R^{(i)}, \quad p' = T_i p_T^{(i)} + R_i p_R^{(i)}. \quad (13)$$

Of course, (\mathbf{u}', p') has stress tensor $\boldsymbol{\sigma}' = T_i \boldsymbol{\sigma}_T^{(i)} + R_i \boldsymbol{\sigma}_R^{(i)}$. Denoting by ${}^t\mathbf{X}$ the transposed value of the vector $\mathbf{X} = (T_1, T_2, T_3, R_1, R_2, R_3)$ it follows from (9)-(13) that

$$\int_S \mathbf{u}' \cdot \boldsymbol{\sigma}' \cdot \mathbf{n} dS = -\mathbf{X} \cdot \mathbf{A} \cdot {}^t\mathbf{X}. \quad (14)$$

If $e'_{ij} = [\partial u'_i / \partial x_j + \partial u'_j / \partial x_i] / 2$ with $u'_i = \mathbf{u}' \cdot \mathbf{e}_i$ we arrive, because (\mathbf{u}', p') obeys (1), that

$$\int_S \mathbf{u}' \cdot \boldsymbol{\sigma}' \cdot \mathbf{n} dS + \sum_{l=1}^2 \int_{\Sigma_l} (-1)^l \mathbf{u}' \cdot \boldsymbol{\sigma}' \cdot \mathbf{e}_3 dS = -2\mu \int_{\Omega} e'_{ij} e'_{ij} d\Omega < 0. \quad (15)$$

Finally, since (\mathbf{u}', p') also fulfills (3) the integrals over Σ_1 and Σ_2 in (15) vanish and (14)-(15) thus shows that $\mathbf{X} \cdot \mathbf{A} \cdot {}^t\mathbf{X} > 0$ for arbitrary vectors \mathbf{X} . Therefore, the real-valued square matrix \mathbf{A} is positive-definite. From the definitions (10) and the identity (7) it is straightforward to prove that \mathbf{A} is also symmetric. Accordingly, the system (11)-(12) admits a unique solution $(\mathbf{U}, \boldsymbol{\omega})$ which is by virtue of (10) obtained by solely determining on the particle's surface the specific tractions $\mathbf{f}_T^{(i)} = \boldsymbol{\sigma}_T^{(i)} \cdot \mathbf{n}$ and $\mathbf{f}_R^{(i)} = \boldsymbol{\sigma}_R^{(i)} \cdot \mathbf{n}$ for $i = 1, 2, 3$.

2.3 Relevant boundary-integral equations and velocity field representation

For source and observation points $\mathbf{y}(y_1, y_2, y_3)$ and $\mathbf{x}(x_1, x_2, x_3)$ located in the domain $\mathcal{D} = \Omega \cup \mathcal{P}$ we consider (for $j = 1, 2, 3$) the Stokes flows $(\mathbf{v}^{(j)}, p^{(j)})$, with stress tensor $\boldsymbol{\sigma}^{(j)}$, such that

$$\mu \nabla^2 \mathbf{v}^{(j)} = \nabla p^{(j)} - \delta_{3d}(\mathbf{x} - \mathbf{y}) \mathbf{e}_j, \quad \nabla \cdot \mathbf{v}^{(j)} = 0 \text{ in } \mathcal{D}, \quad (16)$$

$$(\mathbf{v}^{(j)}, p^{(j)}) \rightarrow (\mathbf{0}, 0) \text{ as } |\mathbf{x} - \mathbf{y}| \rightarrow \infty, \quad (17)$$

$$\mathbf{v}^{(j)} = \mathbf{0} \text{ on } \Sigma_1, \quad (18)$$

$$\mathbf{v}^{(j)} \cdot \mathbf{e}_3 = \mathbf{e}_1 \cdot \boldsymbol{\sigma}^{(j)} \cdot \mathbf{e}_3 = \mathbf{e}_2 \cdot \boldsymbol{\sigma}^{(j)} \cdot \mathbf{e}_3 = 0 \text{ on } \Sigma_2, \quad (19)$$

with $\delta_{3d}(\mathbf{x} - \mathbf{y}) = \delta_d(x_1 - y_1) \delta_d(x_2 - y_2) \delta_d(x_3 - y_3)$ and δ_d the Dirac pseudo-function. Solving (16)-(19) and setting $v_{kj}(\mathbf{x}, \mathbf{y}) = \mathbf{v}^{(j)} \cdot \mathbf{e}_k$ then provides the second-rank and so-called Green tensor $v_{kj}(\mathbf{x}, \mathbf{y}) \mathbf{e}_k \otimes \mathbf{e}_j$ which adequately takes into account the boundaries Σ_1 and Σ_2 . Extending

the approach used for only solid boundaries in Pozrikidis (1992) it is possible to prove, by virtue of (7), the symmetry property

$$v_{kj}(\mathbf{x}, \mathbf{y}) = v_{jk}(\mathbf{y}, \mathbf{x}) \quad (20)$$

and if the pole \mathbf{y} lies in Ω and (\mathbf{u}, p) obeys (1)-(4) to get the flow representation

$$\begin{aligned} u_k(\mathbf{y}) &= [\mathbf{u} \cdot \mathbf{e}_k](\mathbf{y}) = \int_{S \cup \Sigma_1 \cup \Sigma_2} [\mathbf{u} \cdot \boldsymbol{\sigma}^{(j)} \cdot \mathbf{n} - \mathbf{v}^{(j)} \cdot \boldsymbol{\sigma} \cdot \mathbf{n}] dS(\mathbf{x}) \\ &= \int_S [\mathbf{U} + \boldsymbol{\omega} \wedge \mathbf{O}'\mathbf{M}] \cdot \boldsymbol{\sigma}^{(j)} \cdot \mathbf{n} dS(\mathbf{x}) \\ &\quad - \int_S v_{kj}(\mathbf{x}, \mathbf{y}) \mathbf{e}_k \cdot \boldsymbol{\sigma} \cdot \mathbf{n} dS(\mathbf{x}). \end{aligned} \quad (21)$$

Since the pole \mathbf{y} lies outside the particle domain \mathcal{P} where the rigid-body motion $\mathbf{V} = \mathbf{U} + \boldsymbol{\omega} \wedge \mathbf{O}'\mathbf{M}$ is a Stokes flow with constant pressure P , one also obtains the relation

$$\int_S [\mathbf{U} + \boldsymbol{\omega} \wedge \mathbf{O}'\mathbf{M}] \cdot \boldsymbol{\sigma}^{(j)} \cdot \mathbf{n} dS(\mathbf{x}) = -P \int_S \mathbf{v}^{(j)} \cdot \mathbf{n} dS(\mathbf{x}). \quad (22)$$

For \mathbf{y} outside the particle $\mathbf{v}^{(j)}$ is divergence-free in \mathcal{P} and the integrals arising in (22) are thus zero. Recalling (20) and switching the notations \mathbf{y} and \mathbf{x} finally yields for any flow (\mathbf{u}, p) obeying (1)-(4) with arbitrary values of the rigid-body motion $(\mathbf{U}, \boldsymbol{\omega})$ the integral representation

$$u_k(\mathbf{x}) = - \int_S v_{jk}(\mathbf{x}, \mathbf{y}) [\mathbf{e}_k \cdot \boldsymbol{\sigma} \cdot \mathbf{n}](\mathbf{y}) dS(\mathbf{y}), \quad \mathbf{x} \in \Omega \cup S. \quad (23)$$

Note that the above single-layer representation established for \mathbf{x} in the liquid domain indeed also holds by continuity on the boundary S . Exploiting (23) finally makes it possible to solve our problem as follows:

(i) We first compute the required surface tractions $\mathbf{f}_T^{(i)}$ and $\mathbf{f}_R^{(i)}$ on the particle's surface by inverting the following Fredholm boundary-integral equations of the first kind

$$[\mathbf{u}^{(i)} \cdot \mathbf{e}_k](\mathbf{x}) = - \int_S v_{jk}(\mathbf{x}, \mathbf{y}) [\mathbf{f}_L^{(i)} \cdot \mathbf{e}_k](\mathbf{y}) dS(\mathbf{y}) \text{ on } S, \quad (24)$$

obtained by employing (23) on the boundary S for each specific flow $(\mathbf{u}_L^{(i)}, p_L^{(i)})$. The determination of the vectors $\mathbf{f}_L^{(i)}$ on S thus reduces to the treatment of six boundary-integral equations (24) and makes it further possible to compute the unknown rigid-body motion $(\mathbf{U}, \boldsymbol{\omega})$ of the particle by solving the linear system (11)-(12) under the definitions (10). Note that, as outlined in Pozrikidis

(1992), any constant multiple of the unit normal \mathbf{n} on S is an eigensolution of (24). Fortunately, the matrix \mathbf{A} (see (10)) is not sensitive to those eigensolutions and our numerical experiment reveals that for a prescribed mesh on the particle's surface the discretized counterpart of (24) is a well-posed linear system with unique solution.

(ii) If needed, we finally gain the velocity field \mathbf{u} in the liquid domain by using the representation (23) for the previously-obtained surface traction $\boldsymbol{\sigma} \cdot \mathbf{n} = U_i \mathbf{f}_T^{(i)} + \Omega_i \mathbf{f}_R^{(i)}$ on S .

3 Determination of the Green tensor

As established in the previous section, a key issue for the present work consists in determining the Cartesian components $v_{jk}(\mathbf{x}, \mathbf{y})$ of the Green tensor introduced in §2.3. This challenging task, which has not been addressed so far to the authors very best knowledge, is achieved here by mimicking the procedure recently advocated in Jones (2004) when both surfaces Σ_1 and Σ_2 are solid.

3.1 Obtention of the Fourier transform of v_{33}, v_{32}, v_{12} and v_{22}

For symmetry reasons the velocity $\mathbf{v}^{(j)}$ induced by a given pole $\mathbf{y}(y_1, y_2, y_3)$ at the observation point $\mathbf{x}(x_1, x_2, x_3)$ actually depends upon $s_1 = x_1 - y_1, s_2 = x_2 - y_2, x_3$ and y_3 . We thus look at the two-dimensional Fourier transform $\hat{v}_{kj} = \hat{v}_{kj}(\mathbf{q}, x_3, y_3)$ in the $s_1 - s_2$ plane of the coefficient $v_{kj}(\mathbf{x}, \mathbf{y})$ with $\mathbf{q}(q_1, q_2)$ the associated two-dimensional real wave number, as introduced in Jones (2004). Since the calculation of \hat{v}_{kj} follows the lines detailed in this latter paper we here content ourselves with briefly giving the results established for $\hat{v}_{33}, \hat{v}_{k2}$ (with $k = 1, 2, 3$) and the way to deduce from those functions all the coefficients v_{kj} .

Setting $A = (16\mu\pi^2)^{-1}$ and $q = |\mathbf{q}|$, the function \hat{v}_{33} takes the following form

$$\hat{v}_{33} = A[t_{0nn} + t_{1nn}](q, x_3, y_3)/q, \quad (25)$$

$$t_{0nn}(q, x_3, y_3) = (1 + q|x_3 - y_3|)e^{-q|x_3 - y_3|}, \quad (26)$$

$$\begin{aligned} t_{1nn}(q, x_3, y_3) &= S_3 \cosh(qx_3) + S_4 \sinh(qx_3) \\ &\quad + qy_3[S_1 \cosh(qx_3) + S_2 \sinh(qx_3)] \end{aligned} \quad (27)$$

with functions S_1, S_2, S_3 and S_4 , depending on $u = qW$ and $v = qy_2$, determined by enforcing the boundary conditions $\hat{v}_{33} = d\hat{v}_{33}/dx_3 = 0$ at $x_3 = \pm W$ and given in the

Appendix. In a similar fashion, one can also compute the functions \hat{v}_{k2} . Curtailing the details and denoting by i the complex such that $i^2 = -1$, it has been found by a great deal of algebra that

$$\hat{v}_{32} = iAq_2[t_{0np} + t_{1np}](q, x_3, y_3)/q^2, \quad (28)$$

$$t_{0np}(q, x_3, y_3) = -q(x_3 - y_3)e^{-q|x_3 - y_3|}, \quad (29)$$

$$t_{1np}(q, x_3, y_3) = N_3 \cosh(qx_3) + N_4 \sinh(qx_3) + qy_3[N_1 \cosh(qx_3) + N_2 \sinh(qx_3)], \quad (30)$$

$$\hat{v}_{12} = -Aq_1q_2[t_{0pp} + t_{1pp}](q, x_3, y_3)/q^3, \quad (31)$$

$$t_{0pp}(q, x_3, y_3) = t_{0nn}(q, x_3, y_3), \quad (32)$$

$$t_{1pp}(q, x_3, y_3) = M_1 \cosh(qx_3) + M_2 \sinh(qx_3) + qy_3[N_1 \cosh(qx_3) + N_2 \sinh(qx_3)], \quad (33)$$

$$\hat{v}_{22} = A[r_{0pp} + r_{1pp} - \frac{q_2^2}{q^2}(t_{0pp} + t_{1pp})](q, x_3, y_3)/q, \quad (34)$$

$$r_{0pp}(q, x_3, y_3) = 2e^{-q|x_3 - y_3|}, \quad (35)$$

with functions N_m, M_1, M_2 and r_{1pp} dictated by the boundary conditions $\hat{v}_{k2} = d\hat{v}_{k2}/dx_3 = 0$ for $k = 1, 2, 3$ at $x_3 = -W$ and $\hat{v}_{32} = d\hat{v}_{12}/dx_3 = d\hat{v}_{22}/dx_3 = d^2\hat{v}_{23}/dx_3^2 = 0$ at $x_3 = W$. More precisely, one finds that for $u = qW, v = qy_3$ and $w = qx_3$

$$r_{1pp}(q, x_3, y_3) = \frac{2e^{-u}}{\cosh(2u)} \left\{ \cosh v(e^u \sinh w - e^{-u} \cosh w) + \sinh v(e^u \cosh w + e^{-u} \sinh w) \right\} \quad (36)$$

whereas N_m, M_1 and M_2 are provided as functions of (u, v) in the Appendix.

3.2 Final expression and decomposition of the Green tensor

Each component v_{kj} is obtained by taking the inverse Fourier transform of \hat{v}_{kj} . If δ designates the usual Kronecker delta, the final result then reads

$$v_{kj}(\mathbf{x}, \mathbf{y}) = \frac{1}{8\pi\mu} [g_{kj} + r_{kj}](\mathbf{x}, \mathbf{y}), \quad (37)$$

$$g_{kj}(\mathbf{x}, \mathbf{y}) = \frac{\delta_{kj}}{|\mathbf{x} - \mathbf{y}|} + \frac{[(\mathbf{x} - \mathbf{y}) \cdot \mathbf{e}_k][(\mathbf{x} - \mathbf{y}) \cdot \mathbf{e}_j]}{|\mathbf{x} - \mathbf{y}|^3} \quad (38)$$

where one recognizes the free-space Oseen-Burgers Green tensor $g_{kj}\mathbf{e}_k \otimes \mathbf{e}_j$ (see Happel and Brenner (1973)) which prevails in absence of boundaries (case of the unbounded fluid domain) and the occurrence of a regular tensor $r_{kj}\mathbf{e}_k \otimes \mathbf{e}_j$ which permits the obtained Green tensor to comply with the boundary conditions on the plane solid wall and free surfaces Σ_1 and Σ_2 . As in Jones (2004)³, if J_0, J_1 and J_2 designate the usual Bessel functions this additional tensor satisfies

$$r_{11}(\mathbf{x}, \mathbf{y}) = -\frac{1}{2} \int_0^\infty \{J_0(qs)[t_{1pp} - 2r_{1pp}](q, x_3, y_3) + \frac{s_2^2 - s_1^2}{s^2} J_2(qs)t_{1pp}(q, x_3, y_3)\} dq, \quad (39)$$

$$r_{33}(\mathbf{x}, \mathbf{y}) = \int_0^\infty J_0(qs)t_{1nn}(q, x_3, y_3) dq, \quad (40)$$

$$r_{12}(\mathbf{x}, \mathbf{y}) = \frac{s_1 s_2}{s^2} \int_0^\infty J_2(qs)t_{1pp}(q, x_3, y_3) dq, \quad (41)$$

$$r_{13}(\mathbf{x}, \mathbf{y}) = -\frac{s_1}{s} \int_0^\infty J_1(qs)t_{1pn}(q, x_3, y_3) dq, \quad (42)$$

$$t_{1pn}(q, x_3, y_3) = -t_{1np}(q, y_3, x_3), \quad (43)$$

whereas $r_{23}(\mathbf{x}, \mathbf{y})$ is obtained from r_{13} by replacing s_1 with s_2 in (42)-(43), $r_{22}(\mathbf{x}, \mathbf{y})$ is deduced from r_{11} by replacing (s_1, s_2) with $(s_2, -s_1)$ in (39) and the remaining components are given by applying the same symmetry property as (20).

4 Numerical method and results

This section describes the achieved numerical implementation and also provides results for the settling motion of a spherical particle with uniform density ρ_s .

4.1 Numerical implementation

The integrands of the integrals (39)-(42) tend to zero when q becomes large but such a decay becomes very slow as (x_3, y_3) approaches either (W, W) or $(-W, -W)$,

³The misprint occurring for $T_{1,xy}$ in equation (26) in this latter paper is corrected here.

i. e. when both the pole \mathbf{y} and the observation point \mathbf{x} lie in the vicinity of the same boundary Σ_1 or Σ_2 . In such circumstances a dramatic loss of accuracy results if one directly evaluates the integrals (39)-(42) by a usual Gaussian quadrature. We circumvent this difficulty by using the following decompositions

$$t_{1nn} = t'_{1nn} - e^{q(x_3+y_3-2W)} \{q(x_3+y_3-2W) - 1\} + e^{-q(x_3+y_3+2W)} \{2q^2(W+x_3)(W+y_3) + q(2W+x_3+y_3) + 1\}, \quad (44)$$

$$t_{1pn} = t'_{1pn} + q(2W-x_3-y_3)e^{q(x_3+y_3-2W)} - e^{-q(x_3+y_3+2W)} \{2q^2(W+x_3)(W+y_3) + q(x_3-y_3)\}, \quad (45)$$

$$t_{1pp} = t'_{1pp} + e^{q(x_3+y_3-2W)} \{q(x_3+y_3-2W) - 1\} - e^{-q(x_3+y_3+2W)} \{2q^2(W+x_3)(W+y_3) - q(2W+x_3+y_3) - 1\}, \quad (46)$$

$$r_{1pp} = r'_{1pp} - 2e^{q(x_3+y_3-2W)} + 2e^{-q(x_3+y_3+2W)}, \quad (47)$$

where the regularized functions $t'_{1nn}, t'_{1np}, t'_{1pp}$ and r'_{1pp} quickly vanish for q large whatever the value of (x_3, y_3) . We then accurately evaluate the integrals (39)-(42) obtained by replacing the functions $t_{1nn}, t_{1np}, t_{1pp}, r_{1pp}$ with $t'_{1nn}, t'_{1np}, t'_{1pp}$ and r'_{1pp} , respectively by using the change of variable $t = -\log(q)$ and a standard Gaussian quadrature.

Each encountered boundary-integral equation (24) is numerically inverted by employing a standard boundary element technique (see, among others, Bonnet (1999)). For a sake of accuracy, we here resort on the particle's surface to a N -node mesh consisting of isoparametric, curved and triangular boundary elements. When discretized at each nodal point each equation (24) then results in a linear system $\mathbf{M} \cdot \mathbf{X} = \mathbf{Y}$ with fully-populated, real-valued and non symmetric influence $3N \times 3N$ square matrix \mathbf{M} . At that stage the exhibited decomposition (37)-(38) of each Cartesian component v_{kj} into a weakly-singular analytical term g_{kj} and a regular one r_{kj} (evaluated as previously explained) permits us a straightforward and accurate computation of this influence matrix \mathbf{M} . Because this latter issue is standard, we however direct the reader to Pozrikidis (1992) and Bonnet (1999) for further details, especially for the removal of the weakly singular singularity exhibited by g_{kj} . Finally, each arising linear system $\mathbf{M} \cdot \mathbf{X} = \mathbf{Y}$ is solved by Gaussian elimination.

4.2 Numerical results

We confine our attention to the case of a sphere with constant density ρ_s , radius $a < W$ and center $O' = O''$ such that $\mathbf{OO}' \cdot \mathbf{e}_3 + W = h > a$, as illustrated in Fig. 2. Note

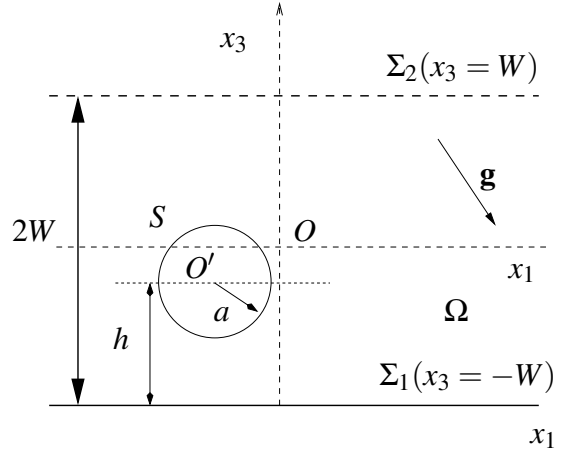


Figure 2 : Case of a solid sphere with radius a , uniform density ρ_s and center $O' = O''$.

that under these notations $h < 2W - a$ whereas $h - a$ is the gap between the sphere's surface and the solid wall Σ_1 . In absence of boundaries the sphere is known to settle (without rotating) parallel to the uniform gravity field \mathbf{g} at the velocity $2a^2(\rho_s - \rho)\mathbf{g}/(9\mu)$. This motion is affected in the present analysis by the sphere's interactions with Σ_1 and/or Σ_2 which clearly depend upon the normalized fluid film thickness $2W/a$ and the particle's location h/a . As shown by symmetries, when $\mathbf{g} = g\mathbf{e}_1$ is parallel to the boundaries \mathbf{U} and $\boldsymbol{\omega}$ are aligned with \mathbf{e}_1 and \mathbf{e}_2 , respectively whereas only $\mathbf{U} \cdot \mathbf{e}_3$ is non-zero if $\mathbf{g} = g\mathbf{e}_3$ is normal to the boundaries. Therefore, by superposition we only compute for $\mathbf{g} \neq \mathbf{0}$ the normalized translational velocity components u, v and normalized angular velocity w defined as

$$u = \frac{9\mu\mathbf{U} \cdot \mathbf{e}_1}{2(\rho_s - \rho)a^2g} \text{ and } w = \frac{9\mu\boldsymbol{\omega} \cdot \mathbf{e}_2}{2(\rho_s - \rho)ag} \text{ if } \mathbf{g} = g\mathbf{e}_1, \quad (48)$$

$$v = \frac{9\mu\mathbf{U} \cdot \mathbf{e}_3}{2(\rho_s - \rho)a^2g} \text{ if } \mathbf{g} = g\mathbf{e}_3. \quad (49)$$

As illustrated in Tab. 1 and Tab. 2, putting $N = 242$ nodal points on the sphere yields a quite sufficient relative accuracy of order of one percent even for the severe case of

Table 1 : Computed normalized velocity components u, w and v using increasingly refined N -node meshes on a sphere located at the center ($O' = O$) of a fluid film of medium thickness: $W = h = 2a$.

N	u	w	v
74	0.685834	0.024189	0.4164102
242	0.683736	0.024437	0.4146364
1058	0.683506	0.024455	0.4144290

Table 2 : Computed normalized velocity components u, w and v using increasingly refined N -node meshes on a sphere located at the center ($O' = O$) of a thin fluid film: $W = h = 1.1a$.

N	u	w	v
74	0.426037	0.057660	0.078630
242	0.423524	0.060454	0.069648
1058	0.423205	0.060439	0.069313

a thin fluid film ($W = h = 1.1a$). All reported computations have thus been performed with $N = 242$.

We first examine the influence of the fluid film thickness $2W$ on the induced velocities u, v and w when the sphere is located either very close to the solid wall Σ_1 with $h = 1.1a$ or very close to the free-surface Σ_2 with $h = 2W - 1.1a$.

The sphere is clearly seen in Fig. 3(a) to settle faster when close to the free surface than when close to the solid wall. Indeed, the no-slip condition on the solid boundary requires a small fluid velocity in it's vicinity whereas the mixed velocity-stress condition on the free surface authorizes larger fluid velocities near it. The sphere translates normal to the boundaries slower than parallel to the wall ($v < u$) in all circumstances. Note also that its interactions with the boundaries slow down the sphere ($u < 1$ and $v < 1$) except when it migrates parallel and close to the free surface with $u = 1$ for a critical fluid film thickness $W_c \sim 2.65a$, $u < 1$ for $W < W_c$ and $u > 1$ for $W > W_c$. In this latter circumstances, the free-surface actually drives the motion of the sphere and makes it move faster than if isolated as it happens for a sphere moving parallel and close to a single free surface (see Lee, Chadwick, and Leal (1979)). The motion of a sphere close to the solid wall is weakly sensitive to the influence of the

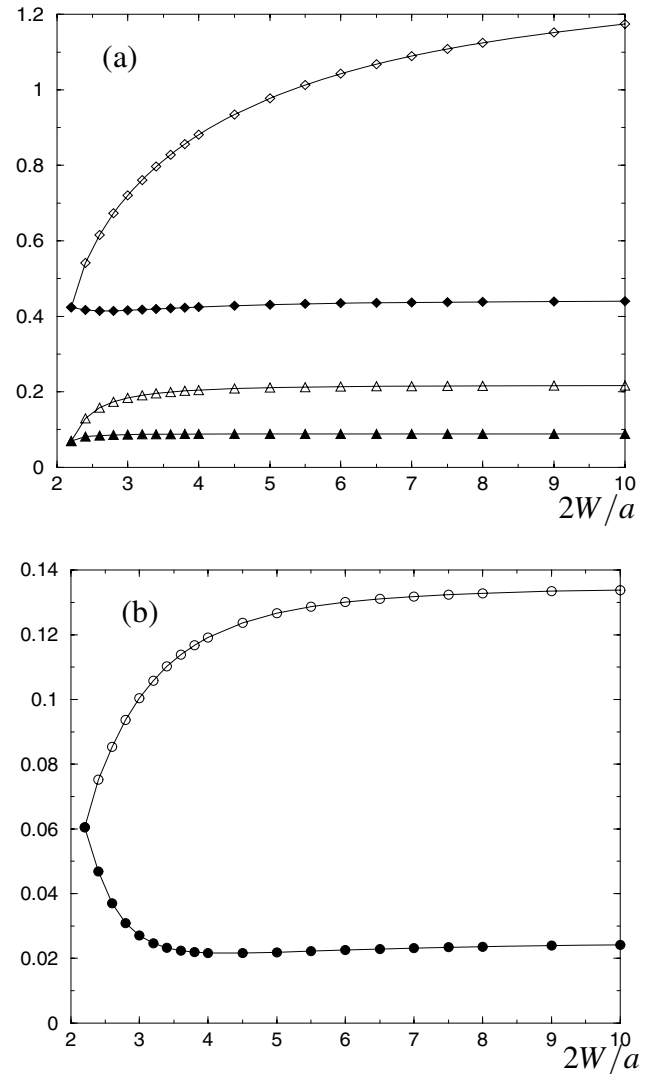


Figure 3 : Normalized velocities u, v and w versus the normalized fluid film thickness $2W/a$ for a sphere close to the solid wall Σ_1 ($h = 1.1a$) or to the free-surface Σ_2 ($h = 2W - 1.1a$). (a) u for a sphere close to Σ_1 (\diamond) or Σ_2 (\diamond) and v for a sphere close to Σ_1 (\blacktriangle) or Σ_2 (\triangle). (b) w for a sphere close to Σ_1 (\bullet) or Σ_2 (\circ).

free surface (see the nearly flat curves for u and v) which actually decays as $(2W/a)^{-2}$. When the sphere is close to the free surface a similar trend is observed for the normal migration (the normalized velocity v exhibits a flat profile versus

$2W/a$ near $2W/a = 10$) but the influence of the solid wall on the parallel motion becomes larger and scales as $(2W/a - 1.1)^{-1}$. As depicted in Fig. 3(b), the interactions with the boundaries also make the sphere rotate

when it settles parallel to the solid wall. The resulting positive angular velocity w is larger when the sphere lies near the free surface than when it is

close to the solid wall whatever the fluid film thickness $2W$.

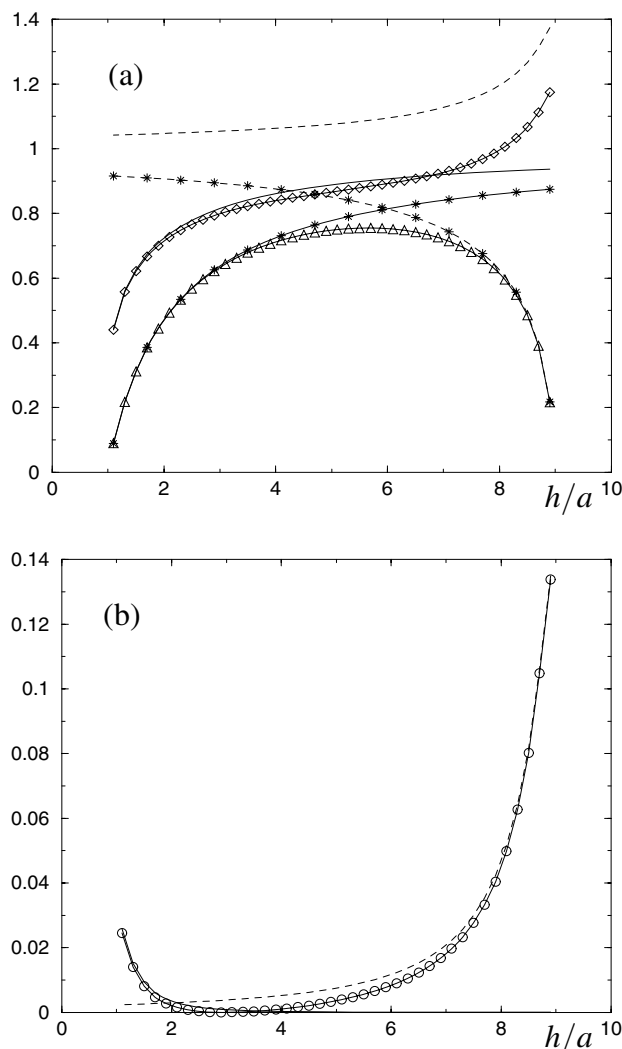


Figure 4 : Normalized velocities u, v and w versus h/a for $W = 5a$. (a) $u(\diamond)$ and $v(\triangle)$. (b) $w(\circ)$. We also plot u, w (solid lines) or v (solid line and symbols $*$) in absence of free surface (when there is only a solid wall) and u, w (dashed curves) or v (dashed line and symbols $*$) in absence of solid wall.

Let us now investigate the influence of the boundaries for a given fluid thickness $2W$ and a sphere not necessarily located very close to Σ_1 or Σ_2 . This is achieved for $2W = 10a$ by plotting in Fig. 4 the normalized ve-

locities u, v and w versus h/a . For comparisons, we also provide the computed values for a single solid wall and a single free surface if one employs the associated Green function given in Blake (1971) and Lee, Chadwick, and Leal (1979), respectively. As previously emphasized, the sphere settles parallel to the boundaries faster ($u > 1$) or slower ($u < 1$) than in an unbounded fluid ($u = 1$) when it lies very close to the solid wall or the free surface, respectively. Accordingly there exists, as seen in Fig. 4(a), a critical value $h_c \sim 8.1a$ at which the wall-sphere and free-surface sphere interactions cancel with $u(h_c) = 1, u < 1$ if $h < h_c$ and $u > 1$ if $h > h_c$. In addition, both the normal velocity v and the angular velocity w are positive and exhibit a maximum and a minimum respectively for different locations h/a of the sphere.

5 Concluding remarks

A new approach has been proposed to accurately determine at a reasonable cpu time cost the slow viscous gravity-driven motion of a solid particle between two plane and parallel solid wall and free surface. The Green tensor associated with these specific boundary conditions is analytically obtained and it is shown how to gain the particle's migration by solely inverting six carefully-selected boundary-integral equations on its surface. The procedure holds for arbitrarily-shaped particles and circumvents determining the fluid flow velocity field. This later however receives a fruitful integral representation which would also permit its straightforward and subsequent computation in the liquid domain. As revealed by our computations, the migration of a sphere deeply depends upon its location, the film fluid thickness and the direction of the gravity field \mathbf{g} . Depending on \mathbf{g} the sphere may either translate parallel to the gravity field (for instance when \mathbf{g} is normal or parallel to the boundaries), as if in an unbounded fluid, or not. In addition, when \mathbf{g} is normal to the boundaries the sphere always moves slower than if isolated whereas when \mathbf{g} is parallel to the boundaries it may either migrates slower, faster or even at the same speed (therefore ignoring the boundaries) than as isolated.

In practice collections of particles are encountered and the liquid may be subject to a prescribed external flow (think, for instance, about linear shear and quadratic Poiseuille flows). Such challenging issues are likely to be adequately addressed by extending the present method to the case of several particles as recently achieved in Pasol

and Sellier (2006) for the sedimentation of a two-particle cluster between two parallel and solid plane walls. Such a task will be pursued in future research to investigate combined particle-particle and particle-wall or particle-free surface interactions. For this purpose we intend to use the method described in Wang and Yao (2005) whenever the number of particles becomes large.

Finally, one should note that the advocated approach would also permit to compute, through the achieved determination of the associated Green tensor, the motion of a bioartificial capsule immersed in a fluid film by mimicking and extending the treatment employed in Dias and Barthes-biesel (2002) for an ellipsoidal capsule moving in a long axisymmetric pore with a hyperbolic entrance.

References

Blake, J. R. (1971): A note on the image system for a Stokeslet in a no-slip boundary. *Proc. Camb. Phil. Soc.*, vol. 70, pp. 303–310.

Bonnet, M. (1999): *Boundary Integral Equation Methods for Solids and Fluids*. John Wiley & Sons Ltd.

Dias, A.; Barthes-biesel, D. (2002): A Geometrically Nonlinear Nine-Node Solid Shell Element Formulation with Reduced Sensitivity to Mesh Distortion. *CMES: Computer Modeling in Engineering & Sciences*, vol. 3, pp. 321–338.

Ganatos, P.; Pepper, R.; Weibaum, S. (1980a): A strong interaction theory for the creeping motion of a sphere between plane parallel boundaries. 1. Perpendicular motion. *J. Fluid Mech.*, vol. 9, pp. 739–753.

Ganatos, P.; Pepper, R.; Weibaum, S. (1980b): A strong interaction theory for the creeping motion of a sphere between plane parallel boundaries. 1. Parallel motion. *J. Fluid Mech.*, vol. 9, pp. 755–783.

Happel, J.; Brenner, H. (1973): *Low Reynolds number hydrodynamics*. Martinus Nijhoff.

Jones, R. B. (2004): Spherical particle in Poiseuille flow between planar walls. *Journal of Chemical Physics*, vol. 121, pp. 483–500.

Lee, S. H.; Chadwick, R. S.; Leal, L. G. (1979): Motion of a sphere in the presence of a plane interface. Part 1. An approximate solution by generalisation of the method of Lorentz. *J. Fluid Mech.*, vol. 93, pp. 705–726.

Li, X.; Pozrikidis, C. (2003): Film flow of a suspension down an inclined plane. *Phil. Trans. R. Soc. Lond.*, vol. A 361, no. 1, pp. 847–869.

Pasol, L.; Sellier, A. (2006): Gravitational motion of a two-particle cluster between two parallel plane walls. *Comptes Rendus Mécanique*, vol. 334, pp. 105–110.

Pozrikidis, C. (1992): *Boundary integral and singularity methods for linearized viscous flow*. Cambridge University Press.

Staben, M. E.; Zinchenko, A. Z.; Davis, R. H. (2003): Motion of a particle between two parallel plane walls in low-Reynolds-number Poiseuille flow. *Physics of Fluids*, vol. 15, pp. 1711–1733.

Wang, H.; Yao, Z. (2005): A New Fast Multipole Boundary Element Method for Large Scale Analysis of Mechanical Properties in 3D Particle-Reinforced Composites. *CMES: Computer Modeling in Engineering & Sciences*, vol. 7, pp. 85–96.

Appendix A: Relevant functions for the green tensor

This Appendix provides the functions S_m, N_m (for $m = 1, \dots, 4$) and M_1, M_2 arising in (27), (30) and (33). For convenience we introduce the new variables $u = qW, v = qY_3$ and functions

$$E_{\pm}(u) = \sinh(u) \cosh(u)_{\pm} u, \quad (50)$$

$$A_{\pm}(u) = u_{\pm}^{\pm} \sinh(u) e^{-u}, \quad (51)$$

$$B(u) = u + \cosh(u) e^{-u}. \quad (52)$$

Under those definitions and through elementary but tedious manipulations it is found that

$$\begin{aligned} E_{-}(2u)S_1 = & -[2u \sinh^2(u)] \cosh v \\ & + 2[\cosh^2(u)B(u) + \sinh(u)e^{-u}E_{+}(u)] \sinh v \\ & - [2 \cosh^2(u)]v \cosh v + [\sinh(2u)]v \sinh v, \end{aligned} \quad (53)$$

$$\begin{aligned} \cosh(u)E_{-}(2u)S_2 = & [2u \sinh^3(u) + E_{-}(2u)e^{-u}] \cosh v \\ & - [2 \sinh(u)(\cosh^2(u)B(u) + \sinh(u)e^{-u}E_{+}(u)) \\ & - E_{-}(2u)e^{-u}] \sinh v \\ & + [\cosh(u) \sinh(2u)]v \cosh v \\ & - [2 \sinh^2(u) \cosh(u)]v \sinh v, \end{aligned} \quad (54)$$

$$\begin{aligned} \cosh^2(u)E_-(2u)S_3 = & - [B(u)E_-(2u) + 2u^2 \sinh^4(u)] \cosh v \\ & + [2u \cosh^2(u) \sinh^2(u)B(u) + 2u \sinh^3(u)E_+(u)e^{-u} \\ & - u \sinh(u)e^{-u} + E_-(2u)] \sinh v \\ & - [2u \sinh^2(u) \cosh^2(u)]v \cosh v \\ & + \cosh(u)[E_-(2u)e^{-u} + 2u \sinh^3(u)]v \sinh v, \end{aligned} \quad (55)$$

$$\begin{aligned} M_3^1 = & -E_-(2u) + \sinh(2u)[\sinh^2(u) + u \sinh(2u)] \\ & - 2 \sinh^2(u)E_-(u), \end{aligned} \quad (62)$$

$$\begin{aligned} \sinh(u)E_-(2u)S_4 = & [u^2 \sinh(2u) \sinh(u)] \cosh v \\ & - [e^{-u}(1 + u)E_-(2u) + 2u \cosh^3(u)B(u) \\ & + u \sinh^2(u)e^{-u}E_+(u)] \sinh v \\ & + [e^{-u}E_-(2u) + 2u \cosh^3(u)]v \cosh v \\ & - [2u \sinh(u) \cosh^2(u)]v \sinh v, \\ E_-(2u)N_1 = & -[A_-(2u) + u \sinh(u)] \cosh v \\ & + [2u \sinh^2(u) - \sinh(2u)] \sinh v \\ & - [\sinh(2u)]v \cosh v + [2 \cosh^2(u)]v \sinh v, \end{aligned} \quad (56)$$

$$\begin{aligned} M_1^2 = & E_-(2u)A_+(u) + E_+(u)[A_-(2u) + u \sinh(2u)] \\ & - [\cosh^2(u) + u \sinh(2u)][2u \cosh^2(u) - \sinh(2u)], \end{aligned} \quad (64)$$

$$\begin{aligned} M_2^2 = & E_-(2u)e^{-u}[u \cosh(u) - \sinh(u) - u \sinh(u)] \\ & - E_+(u)[2u \sinh^2(u) - \sinh(2u)] \\ & - [\cosh^2(u) + u \sinh(2u)][A(2u) - u \sinh(2u)], \end{aligned} \quad (65)$$

$$\begin{aligned} E_-(2u)N_2 = & [2u \cosh^2(u) - \sinh(2u)] \cosh v \\ & + [A_-(2u) - u \sinh(2u)] \sinh v \\ & + [2 \sinh^2(u)]v \cosh v - [\sinh(2u)]v \sinh v, \end{aligned} \quad (57)$$

$$\begin{aligned} M_3^2 = & -E_-(2u)e^{-2u} + E_+(u) \sinh(2u) \\ & - 2 \sinh^2(u)[\cosh^2(u) + u \sinh(2u)], \end{aligned} \quad (66)$$

$$\begin{aligned} E_-(2u)N_3 = & [2u \sinh^2(u) - u^2 \sinh(2u)] \cosh v \\ & + [uE_-(2u) - 2u \sinh^2(u)E_-(u) \\ & - u \sinh^2(u) \sinh(2u)] \sinh v \\ & + [2 \sinh^2(u) \cosh(2u) - u \sinh(2u) - E_-(2u)]v \cosh v \\ & + [2u \sinh^2(u)]v \sinh v, \end{aligned} \quad (58)$$

$$\begin{aligned} M_4^2 = & -E_-(2u) - 2 \cosh^2(u)E_+(u) \\ & + \sinh(2u)[\cosh^2(u) + u \sinh(2u)], \end{aligned} \quad (67)$$

$$\begin{aligned} E_-(2u)N_4 = & [2u \cosh^2(u)E_+(u) - uE_-(2u) \\ & + u \cosh^2(u) \sinh(2u)] \cosh v \\ & + [2u \cosh^2(u) - u^2 \sinh(2u)] \sinh v \\ & + [E_-(2u) - 2 \cosh^2(u) \cosh(2u) - u \sinh(2u)]v \sinh v \\ & + [2u \cosh^2(u)]v \cosh v \end{aligned} \quad (59)$$

and upon introducing the following functions

$$\begin{aligned} M_1^1 = & E_-(2u)e^{-u}[u \sinh(u) - \cosh(u) - u \cosh(u)] \\ & + [A(2u) + u \sinh(2u)][\sinh^2(u) + u \sinh(2u)] \\ & - E_-(2u)[2u \cosh^2(u) - \sinh(2u)], \end{aligned} \quad (60)$$

$$\begin{aligned} M_2^1 = & E_-(2u)e^{-u}[u \sinh(u) + \cosh(u) + u \cosh(u)] \\ & - [\sinh^2(u) + u \sinh(2u)][2u \sinh^2(u) - \sinh(2u)] \\ & - E_-(2u)[A_-(2u) - u \sinh(2u)], \end{aligned} \quad (61)$$

one also arrives at

$$\begin{aligned} \cosh(2u)E_-(2u)M_1 = & M_1^1 \cosh v + M_2^1 \sinh v \\ & + M_3^1 v \cosh v + M_4^1 v \sinh v, \end{aligned} \quad (68)$$

$$\begin{aligned} \cosh(2u)E_-(2u)M_2 = & M_1^2 \cosh v + M_2^2 \sinh v \\ & + M_3^2 v \cosh v + M_4^2 v \sinh v. \end{aligned} \quad (69)$$